Stem Cell Research (2015) 14, 114–129

Available online at www.sciencedirect.com

ScienceDirect

www.elsevier.com/locate/scr

Detection of mouse endogenous type B astrocytes migrating towards brain lesions

Gema Elvira[a], Isabel García[b,c], Juan Gallo[b], Marina Benito[d,1], Paula Montesinos[e], Esther Holgado-Martin[f], Angel Ayuso-Sacido[f], Soledad Penadés[b,c], Manuel Desco[d,e], Augusto Silva[a,2], Jose A. Garcia-Sanz[a,*]

[a] *Centro de Investigaciones Biológicas (CIB-CSIC), Madrid, Spain*
[b] *Laboratory of Glyconanotechnology, CICbiomaGUNE, San Sebastian, Spain*
[c] *CIBER-BBN, San Sebastian, Spain*
[d] *Medicina y Cirugía Experimental, Hospital General Universitario Gregorio Marañón, CIBERSAM, Madrid, Spain*
[e] *Department of Bioengineering and Aerospace Engineering, Universidad Carlos III, Madrid, Spain*
[f] *Centro Integral Oncológico Clara Campal (CIOCC) and Instituto de Medicina Molecular Aplicada (IMMA), Hospital de Madrid Foundation, Madrid, Spain*

Received 2 February 2014; received in revised form 17 November 2014; accepted 24 November 2014
Available online 3 January 2015

Abstract Neuroblasts represent the predominant migrating cell type in the adult mouse brain. There are, however, increasing evidences of migration of other neural precursors. This work aims at identifying *in vivo* endogenous early neural precursors, different from neuroblasts, able to migrate in response to brain injuries. The monoclonal antibody Nilo1, which unequivocally identifies type B astrocytes and embryonic radial glia, was coupled to magnetic glyconanoparticles (mGNPs). Here we show that Nilo1–mGNPs in combination with magnetic resonance imaging in living mice allowed the *in vivo* identification of endogenous type B astrocytes at their niche, as well as their migration to the lesion site in response to glioblastoma, demyelination, cryolesion or mechanical injuries. In addition, Nilo1$^+$ adult radial glia-like structures were identified at the lesion site a few hours after damage. For all damage models used, type B astrocyte migration was fast and orderly. Identification of Nilo1$^+$ cells surrounding an induced glioblastoma was also possible after intraperitoneal injection of the antibody. This opens up the possibility of an early identification of the initial damage site(s) after brain insults, by the migration of type B astrocytes.

Abbreviations: CC, corpus callosum; LPC, lysophosphatidilcholine; mGNPs, magnetic glyconanoparticles; GBM, human glioblastoma; MRI, magnetic resonance imaging; Nilo1–mGPs, monoclonal antibody coupled to magnetic glyconanoparticles; OB, olfactory bulb; PF, paraformaldehyde; RMS, rostral migratory stream, RG, radial glia; SGZ, subgranular zone; SVZ, subventricular zone.

* Corresponding author at: CIB-CSIC, Ramiro de Maeztu 9, E-28040 Madrid, Spain. Fax: +34 915360432.
E-mail address: jasanz@cib.csic.es (J.A. Garcia-Sanz).
[1] Present address: Department of Epidemiology, Atherothrombosis and Imaging Spanish National Cardiovascular Research Centre (CNIC), Madrid, Spain.
[2] Present address: R&D Department, Althia Health SL, Madrid, Spain.

http://dx.doi.org/10.1016/j.scr.2014.11.006
1873-5061/

Introduction

Neural stem cells in adult rodents are mainly restricted to the niches at the subventricular zone (SVZ) in the lateral ventricles and the subgranular zone (SGZ) in the hippocampal dentate gyrus (Doetsch et al., 1999; Palmer et al., 1997; Reynolds and Weiss, 1992; Richards et al., 1992). In the adult SVZ, type B cells express glial markers, have astrocyte characteristics, bundles of intermediate filaments and multiple processes (Doetsch et al., 1999; Peters et al., 1991), and generate neuroblasts (type A cells, neuronal precursors) through a highly proliferative transit amplifying population (type C cells) (Doetsch et al., 1999; Kriegstein and Alvarez-Buylla, 2009). The cell bodies of type B astrocytes are generally located under the ependymal layer of the lateral ventricles, have short processes that extend through it, with small apical endings on the ventricle, in addition to frequently tangentially oriented long basal processes with specialized end feet on blood vessels (Kriegstein and Alvarez-Buylla, 2009; Mirzadeh et al., 2008). Thus, adult SVZ B cells, similarly to the radial glia (RG) during development, retain an apical–basal polarity and are part of the ventricular epithelium (Kriegstein and Alvarez-Buylla, 2009). In fact, although the radial glia disappears postnatally by transformation into parenchymal astrocytes, some radial glial cells persist within the adult SVZ hidden among astrocytes of the glial tubes. This modified radial glia belongs to the astroglial lineage (type B cells) and maintains self-renewal potential and pluripotency, the two stem cell characteristics (Bonfanti and Peretto, 2007; Gubert et al., 2009; Sundholm-Peters et al., 2004).

It is well documented the migration of adult neuroblasts in a pathway known as rostral migratory stream (RMS), in longitudinal clusters from their SVZ niche towards the olfactory bulb (OB), where dying neurons should be replaced (Doetsch et al., 1999; Doetsch and Alvarez-Buylla, 1996; Lois and Alvarez-Buylla, 1994; Lois et al., 1996). In addition, migration of cells from SVZ towards non-olfactory bulb regions in the adult has been reported on several disease or injury models (Arvidsson et al., 2002; Cantarella et al., 2008; Nakatomi et al., 2002; Thored et al., 2006). Surgical RMS disruption led to migration of BdrU$^+$PSA-NCAM$^+$ cells from the SVZ into the anterior olfactory nucleus, the frontal cortex and the *striatum* (Alonso et al., 1999; Jankovski et al., 1998). In addition, in response to an induced brain tumor, the migration of endogenous neuroblasts towards the lesion site could be followed *in vivo* by MRI (Elvira et al., 2012). Although DCX$^+$ neuroblasts are thought to be the major migratory SVZ cells, type C cells might migrate as well (Aguirre and Gallo, 2004). Many of the migration experiments have been done using BrdU-labeled cells, where some, but not all the labeled cells were neuroblasts (Arvidsson et al., 2002; Cantarella et al., 2008; Nakatomi et al., 2002; Thored et al., 2006; Gotts and Chesselet, 2005; Sundholm-Peters et al., 2005). Indeed, several reports suggest that other precursor cells from the SVZ are able to migrate towards a brain lesion site. For instance, on transgenic mice expressing a nestin driven green fluorescent protein (GFP), in response to a glioblastoma, the GFP$^+$ cells surrounding the brain tumor were actively dividing (Ki67$^+$), mushashi$^+$, glial precursors (NG2$^+$), GFAP$^+$, PSA-NCAM$^+$ or DCX$^+$. These phenotypes at the lesion site are compatible with the migration of committed and non-committed precursors (Glass et al., 2005). Time-lapse experiments showed that among the nestin-eGFP$^+$ cells in the SVZ, there were type C cells, GFAP$^+$ cells, neuroblasts, ependymal cells and microglia, where a high percentage of motile nestin-eGFP$^+$ cells were DCX$^-$ (Nam et al., 2007). Taken together, these data suggest that DCX$^+$ neuroblasts do not represent the only motile SVZ-derived cells in the postnatal mouse brain. In cortical injuries, NG2$^+$ cells, Nestin$^+$ GFAP$^+$ cells or SVZ cells able to differentiate into glia were identified in the vicinity of the lesion site at different time points (Glass et al., 2005; Goings et al., 2004; Picard-Riera et al., 2002; Holmin et al., 1997).

We hypothesized that type B astrocytes might be among the other SVZ-derived cell types able to migrate in response to a damage insult. In this study we used Nilo1, a previously characterized mAb that identifies early neural progenitors in the SVZ niche (Del Valle et al., 2010), demonstrating that Nilo1$^+$ cells showed an immunophenotype and subependymal localization compatible with B astrocytes. After coupling Nilo1 mAb to magnetic nanoparticles, we followed by MRI and confirmed by immunohistochemistry the fast mobilization of B astrocytes towards the lesion site, as a trait shared by different brain injuries in adult mice.

Materials and methods

Animals

Experiments involving animals were performed in compliance with the European Union and Spanish laws (Council Directive 86/609/EEC) and approved by the CSIC Committee of Animal Experimentation. For these experiments, 6–8 week old C57Bl/6J mice (males), bred and housed in our animal facility under standard conditions were used. Surgery was performed under anesthesia, and efforts were made to minimize suffering of the animals.

Antibodies

Nilo1 and Nilo2 mAbs were generated by the fusion of hamster B cells and the mouse myeloma X63Ag8, as described (Del Valle et al., 2010). Purification of Nilo1 and Nilo2, biotinylation and Cy5 labeling was from ProteinTools (CNB-CSIC, Madrid, Spain). Commercial antibodies and other reagents are described in Supplementary material Table S1.

Characterization of the protein G-magnetic glyconanoparticles (mGNPs) and coupling to Nilo1

Water-soluble magnetic glyconanoparticles, consisting on a magnetic core (4 nm of diameter) covered with a 1 nm gold shell and coated with carbohydrates and an amphiphilic linker ended in a carboxyl group, were prepared and characterized as previously described (Gallo et al., 2010). Recombinant protein G was covalently immobilized to these particles, which enabled the subsequent capture of IgG antibodies (Gallo et al., 2011; García et al., 2011). Characterization of protein G-glyconanoparticles (mGNPs)

including size and T2* estimation was made as described (Elvira et al., 2012). mGNPs (100 μg) were incubated 5 h at 4 °C with Nilo1 mAb (135 μg) in 0.1 M glycine buffer pH 9.0 on a final volume of 50 μl. Characterization of the amount and functionality of the coupled antibody was made as described (Elvira et al., 2012).

Cell culture

CT-2A mouse astrocytoma (a gift from Prof. T.N. Seyfried, Boston, MA, USA), and GFP-CT-2A (a gift from A. Martinez, I. Cajal, CSIC, Madrid, Spain) (Martinez-Murillo and Martinez, 2007), were grown in RPMI medium, 10% heat-inactivated fetal bovine serum in 5% CO_2 at 37 °C and 95% humidity.

Isolation and culture of cancer-initiating cells from human glioblastoma samples

Glioblastoma (GBM) Tumor Stem Cells were isolated from 4 different human fresh GBM samples. Tissue samples were obtained from patients operated at the Neurosurgery department, Hospital la Fe, Spain. Permission for using this material was obtained from the ethical review board in Hospital la Fe, and written informed consent was obtained from patients. GBM Tumor Stem Sells were cultured in media containing: DMEM/F-12 (Gibco, 11039021) with Non-Essential Amino Acids (10 mM; Gibco, 11140), Hepes (1 M; Gibco, 15630), D-Glucose 45% (Sigma, G8769), BSA-F5 7.5% (Gibco, 15260), Sodium Pyruvate (100 mM; Gibco, 11360), L-Glutamine (200 mM; Gibco), Antibiotic–Antimycotic (100×; Gibco, 15240), N-2 Supplement (100×; Gibco, 17502), Hydrocortisone (1 μg/μl; Sigma, H0135), Tri-iodothyronine (100 μg/ml; Sigma, T5516), EGF (50 ng/μl; Sigma, E9644), bFGF (25 ng/μl; Sigma, F0291) and Heparin (1 ng/μl).

Surgical procedures

Mice were anesthetized intraperitoneally with 100 mg/kg of ketamine and 10 mg/kg of xylacine, their heads were immobilized on a stereotaxic frame and intracranially injected with 1 μl of Nilo1–mGNPs in the right *striatum* at coordinates +0.9 mm anterior, +0.75 mm lateral, and −2.75 mm ventral from bregma point. In control animals, PBS buffer was injected. Brain fixations were performed on anesthetized mice by transcardiac perfusion with 4% paraformaldehyde (PF) in 0.1 M phosphate buffer (fixation buffer). Brains were extracted and post-fixed overnight at 4 °C in fixation buffer and cryoprotected in fixation buffer with 30% sucrose for two days at 4 °C before freezing at −80 °C. Fixed brains were cut with a cryostat (25 μm thick) and slices were maintained at −20 °C in 30% (v/v) glycerol, 30% (v/v) etilenglicol, PB 0.1 M pH 7.4 until analyzed.

Tumors were generated by grafting 10^2–2×10^5 CT-2A (or GFP-CT-2A) cells intracranially at stereotaxic coordinates +0.1 mm anterior, −2.25 mm lateral, and −2.70 mm ventral into the right *caudate putamen*, in 1 μl of PBS (n = 6 for MRI analyses).

Demyelination was induced by injecting 1 μl of 2% LPC in PBS near the *corpus callosum*, at stereotaxic positions +1 mm anterior, −1 mm lateral, and −2 mm ventral from bregma point, on anesthetized mice. Mice (n = 6) were sacrificed 7 or 25 days later.

Mechanical injuries were made on anesthetized mice by inserting a Hamilton needle by stereotaxic surgery (coordinates +0.9 mm anterior, +0.9 mm lateral, −2.75 mm ventral refereed to bregma point) (n = 6). In some mice, the lesion site was labeled by nigrosine (0.5 μl i.c. containing 0.5 ng/μl in sterile PBS). Mice were sacrificed one to three days later.

The cryolesion was generated by applying for 10 s a dry ice pellet onto the left frontoparietal bone of anesthetized mice. Mice (n = 5) were sacrificed three days later.

Magnetic resonance imaging

MRI studies were performed on a Bruker Biospec 70/20 scanner using a combination of a linear coil (for transmission) with a 4-element mouse head phased array coil (for reception). Animals were anesthetized with sevofluorane (5% for induction and 2% for maintenance) and placed in an MRI-adapted stereotaxic holder. Respiration and body temperature were continuously monitored. MRI acquisition protocol included an initial flash sequence (repetition time: 100 ms, echo time: 6 ms, field of view: 4 cm, matrix: 128 × 128) to center the Field of View (FOV), followed by a shimming procedure applied to a region of interest covering the head (FOV = 3 × 2 × 2 cm, matrix = 64 × 64 × 64) based on a Field Map sequence (TR = 20 ms, TE = 1.43 and 5.42 ms).

As an anatomical reference, a T2-weighted axial study (TR = 2500 ms; TE, 33 ms; $\alpha = 180°$; FOV = 2 × 2 cm; matrix = 256 × 256; slice thickness = 0.5 mm, 15 slices to cover the whole brain) was used and nanoparticles were detected and tracked with a T2*-weighted 3D multi gradient echo

Figure 1 Nilo1 mAb identifies type B astrocytes in the adult brain, as well as embryonic radial glia. Immunohistochemistry of subventricular zone from wild type mice by confocal microscopy showing A, double staining with Nilo1 and Sox2, Nestin, GFAP or a triple labeling Nilo1, GFAP and Nestin, indicating that the $Nilo1^+$ cells are positive for these markers. Single and double stainings for these panels are shown in Supplemental Fig. S1. B, $Nilo1^+$ cells are $CD24^-$ and had a subependymal localization. Cells labeled with a short pulse of BrdU (50 mg/kg, 1 h before sacrifice) expressing high levels of Pax6 (see arrows), corresponding to the C population are different from $Nilo1^+$ cells (middle panels) and from neuroblasts ($Nilo2^+$ cells, right panel). C, Double staining with Nilo1 and Nilo 2 demonstrating that $Nilo1^+$ cells are different form $Nilo2^+$ cells (neuroblasts). D, Immunohistochemistry of fixed brains (telencephalic cortex) from E10 mouse embryos double stained with Nilo1 and either nestin or vimentin. Nuclei were counterstained with DAPI. LV, lateral ventricle. V, ventricle. P, pial surface. Scale bars: 50 μm. Localization of this region on the mouse embryo is shown in Supplemental Fig. S3). E, Human primary glioblastoma growing *in vitro* as neurospheres was stained with Nilo1 mAb and revealed with a secondary FITC mouse IgG anti-hamster Ig (green) (left) and counterstained with DAPI (middle). The merged picture is seen on the right panels (controls and the staining of other 4 human glioblastoma cell lines are shown in Supplemental Fig. S4).

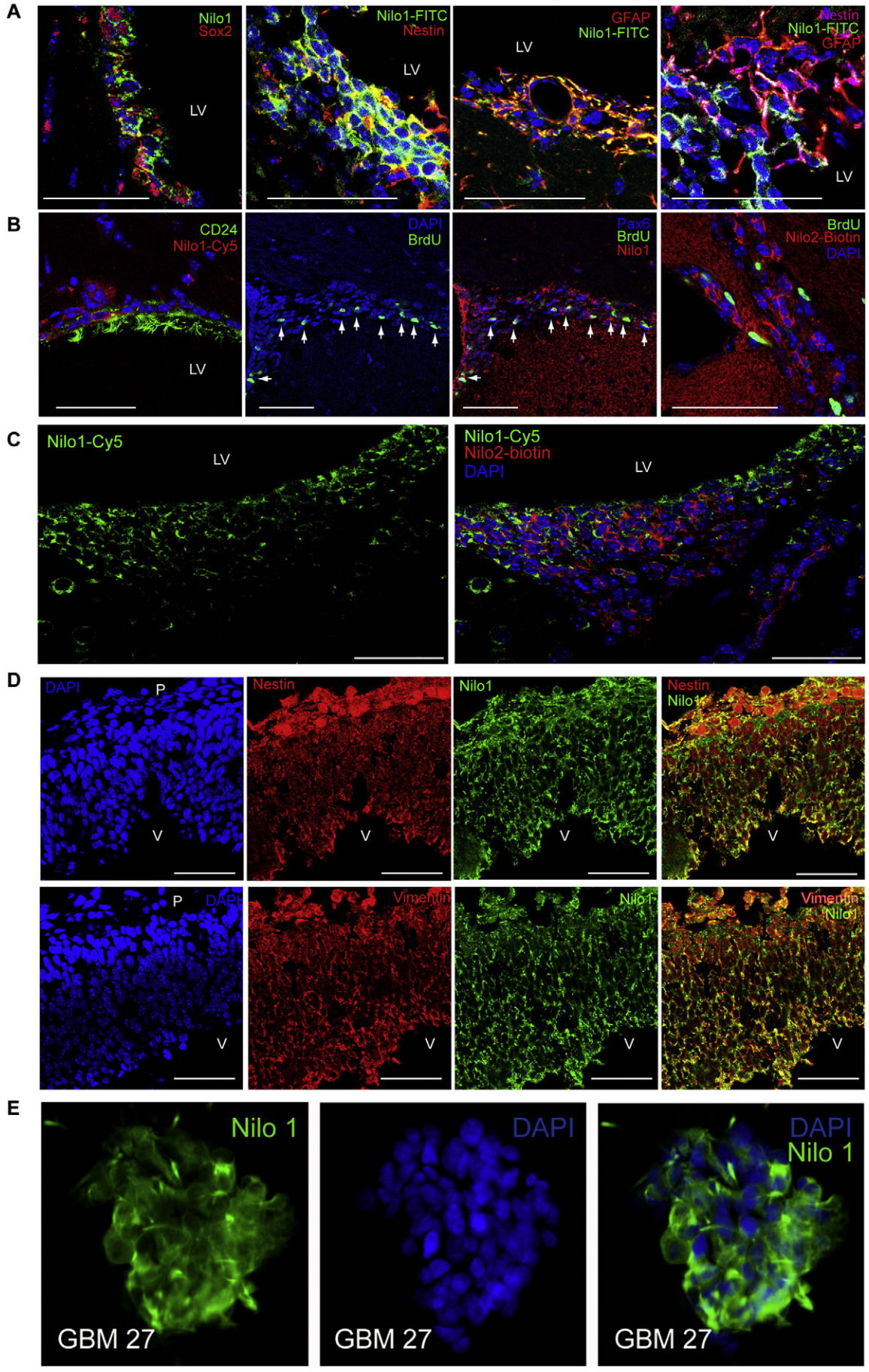
A
Nilo1
Sox2
LV
Nilo1-FITC
Nestin
LV
GFAP
Nilo1-FITC
LV
Nestin
Nilo1-FITC
GFAP
LV
B
CD24
Nilo1-Cy5
LV
DAPI
BrdU
Pax6
BrdU
Nilo1
BrdU
Nilo2-Biotin
DAPI
C
Nilo1-Cy5
LV
Nilo1-Cy5
Nilo2-biotin
DAPI
LV
D
DAPI
P
V
Nestin
V
Nilo1
V
Nestin
Nilo1
V
P
DAPI
V
Vimentin
V
Nilo1
V
Vimentin
Nilo1
V
E
Nilo 1
GBM 27
DAPI
GBM 27
DAPI
Nilo 1
GBM 27

(MGE) sequence (TR = 200 ms; 8 echoes, TE = 10 to 45 ms; echo spacing = 5 ms; $\alpha = 15^{\circ}$; FOV = 1.6 × 1.6 × 1.5 cm; matrix = 192 × 96 × 96).

To increase the signal-to-noise ratio (SNR) and improve image contrast, the different echo images from the MGE sequence were added (in magnitude). To display the results, the tumor area was manually segmented on the T2 axial scans and transferred to the MGE image.

Immunological analyses and staining procedures

Single cell suspensions from cultured neurospheres were attached onto Matrigel Basement Membrane Matrix Growth Factor Reduced (BD Pharmingen) pre-coated coverslips with diluted in culture media (1:20 v/v) as described (Elvira et al., 2012). Cells were fixed with 4% PF in PBS buffer for 15 min at RT. Quenching was performed by adding 0.1 M glycine pH 7.4 for 15 min at RT. After three PBS washes, blocking was performed by incubating the coverslips with 10% goat serum in PBS during 1 h at RT. Fixed cells were incubated overnight with Nilo1–mGNPs or purified Nilo1 mAb at 4 °C. After three PBS washes, cells were incubated with anti-Ha-FITC secondary antibody 1:100 for 1 h.

To assess whether MRI signals corresponded to labeled type B astrocytes, brains from mice used in MRI analyses were fixed and cryopreserved for cryostat sectioning in a plane parallel to that of axial MR imaging. Serial 20–25 μm thick frozen sections were collected through the entire mouse brain. Anatomical landmarks such as *corpus callosum*, lateral ventricles opening, shape and anterior commisure of the brain were used for the spatial alignment of MRI and immunohistochemical sections.

Brain sections of wild type mice or mice intracranially injected with Nilo1–mGNPs were blocked with 10% mouse serum in PBS during 1 h at RT and stained with the appropriate antibodies (Supplemental Table S1). For the identification of Nilo1^{+} cells on Nilo1–mGNP injected mice, anti-Ha-FITC (1:100) or, alternatively, anti-hamster biotin (1:100) followed by streptavidin-A488 (1:400) or streptavidin-Texas Red (1:400) was used. Coverslips were mounted with an anti-fade (Mowiol488), counterstained with either DAPI or Hoechst 33342. Images were collected with a Leica TCS-SP5-AOBS confocal microscope (Mannheim, Germany). Detection ranges were set to eliminate crosstalk between fluorophores.

For *in vivo* identification of Nilo1^{+} cells surrounding the brain tumor, mice were intraperitoneally injected with Nilo1 ascites at 10 μg/g of body weight one week after stereotaxic injection of 100 GFP-CT-2A cells. Mice were sacrificed 24 h later and 25 μm sections of fixed brains were analyzed using a secondary Cy5.5-labeled anti-hamster antibody.

Short BrdU labeling *in vivo*. Mice were intraperitoneally injected with a single dose of BrdU (50 mg/kg). Mice were sacrificed 1 h later and 25 μm cryostate sections were collected. Fixed brain sections were denatured with 2 N HCl in PBS, 0.3% Triton X-100 (PBST) during 30 min at 37 °C. After PBST washes, sections were blocked with 10% goat serum in PBST and incubated with a secondary FITC-labeled anti-BrdU antibody during 24 h at 4 °C. The Pax6^{high} BrdU^{+} population labeled with this protocol represents the type C transit amplifying progenitors (Aguirre and Gallo, 2004; Kim et al., 2009; Parras et al., 2004). These samples were additionally stained with either Nilo1 or Nilo2 mAbs.

C57Bl/6 mouse embryos were obtained in E10 development stage, fixed by immersion in fixation buffer overnight at 4 °C and cryoprotected in fixation buffer with 30% sucrose for two days at 4 °C before freezing in OCT blocks. Cryostat sections of the embryos were mounted in poly-lysine slides and maintained at −20 °C until analyzed (histology service in CNB-CSIC, Madrid, Spain). Radial glia was identified by using vimentin and nestin antibodies in a Leica TCS-SP5-AOBS confocal microscope (Mannheim, Germany). Images of E10 mouse embryo used to compose overview used in Supplemental Fig. S1 were collected in a Leica AF6000 LX Live Cell Imaging microscope (Mannheim, Germany).

Flow cytometry

Single cell suspensions from neurospheres were obtained after incubation with accutase (5 min, 37 °C). Unspecific

Figure 2 Nilo1–mGNPs revealed MRI hypointense signals in brain tumor sites. A, Cartoon representing Nilo1–mGNPs. The nanoparticles were made of a magnetic Fe_3O_4 core, covered by a gold shell (Au) and subsequently coated with carbohydrates and a carboxyl-ending linker to which Protein G was coupled and Nilo1 mAb bound. B, *In vivo* identification of SVZ Nilo1^{+} cells in mice intracranially injected with Nilo1–mGNPs. Brain sections were directly incubated with a secondary biotinylated anti-hamster Ig antibody and revealed with streptavidin A488. DAPI was used to counter-stain nuclei. Scale bar: 25 μm. C, Fluorescence confocal microscopy of Nilo1–mGNPs (top) and Nilo1 mAb (bottom) labeled neurosphere cells grown in Matrigel™. DAPI was used to counter-stain nuclei. Scale bar: 25 μm. D, Flow cytometry analyses of SVZ-derived neurosphere cells stained with Nilo1–mGNPs (light gray) or Nilo1 alone (dark gray) both revealed with a fluorescent secondary antibody. Cells incubated with the secondary antibody in the absence of Nilo1 were used as negative control (black line). E, Schematic representation of the injection sites for the CT-2A astrocytoma cells (left hemisphere, d0) and Nilo1–mGNPs contralaterally in a more rostral position. F, Experimental schedule where Nilo1–mGNPs injection day is indicated with an arrowhead and MRI acquisitions are shown with asterisks, before (empty) or after nanoparticle injection (filled). G, Axial view of T2 MRI image of mouse injected with CT-2A cells (d0) and Nilo1–mGNPs. Dotted line was drawn delimiting the tumor mass. H, Representative T2* MRI study of mice injected with CT-2A cells (d0) and Nilo1–mGNPs (n = 3). Axial, coronal and sagittal views just before (−1 h) or 3 h, 24 h, 48 h after nanoparticle injection. Inset in axial panel at 3 h shows the injection site of Nilo1–mGNPs (a more rostral position than the CT-2A injection site). I, Quantification of MRI signal intensity changes from H. The increase in the accumulation of nanoparticles surrounding the tumor is translated as a drop in the mean signal intensity in the region of interest. The controls are shown in Supplementary Fig. S5.

antibody binding was blocked with PBS, 10% goat serum, 3% BSA, 0.0025% NaN_3 for 30 min at 4 °C. An excess of Nilo1–mGNPs was added to the cell suspension and incubated for 1 h at 4 °C. Cells with purified Nilo1 were incubated as a positive control. After PBS washes, cell suspensions were stained with anti-Ha-FITC (1:100 diluted in PBS, 5% BSA,

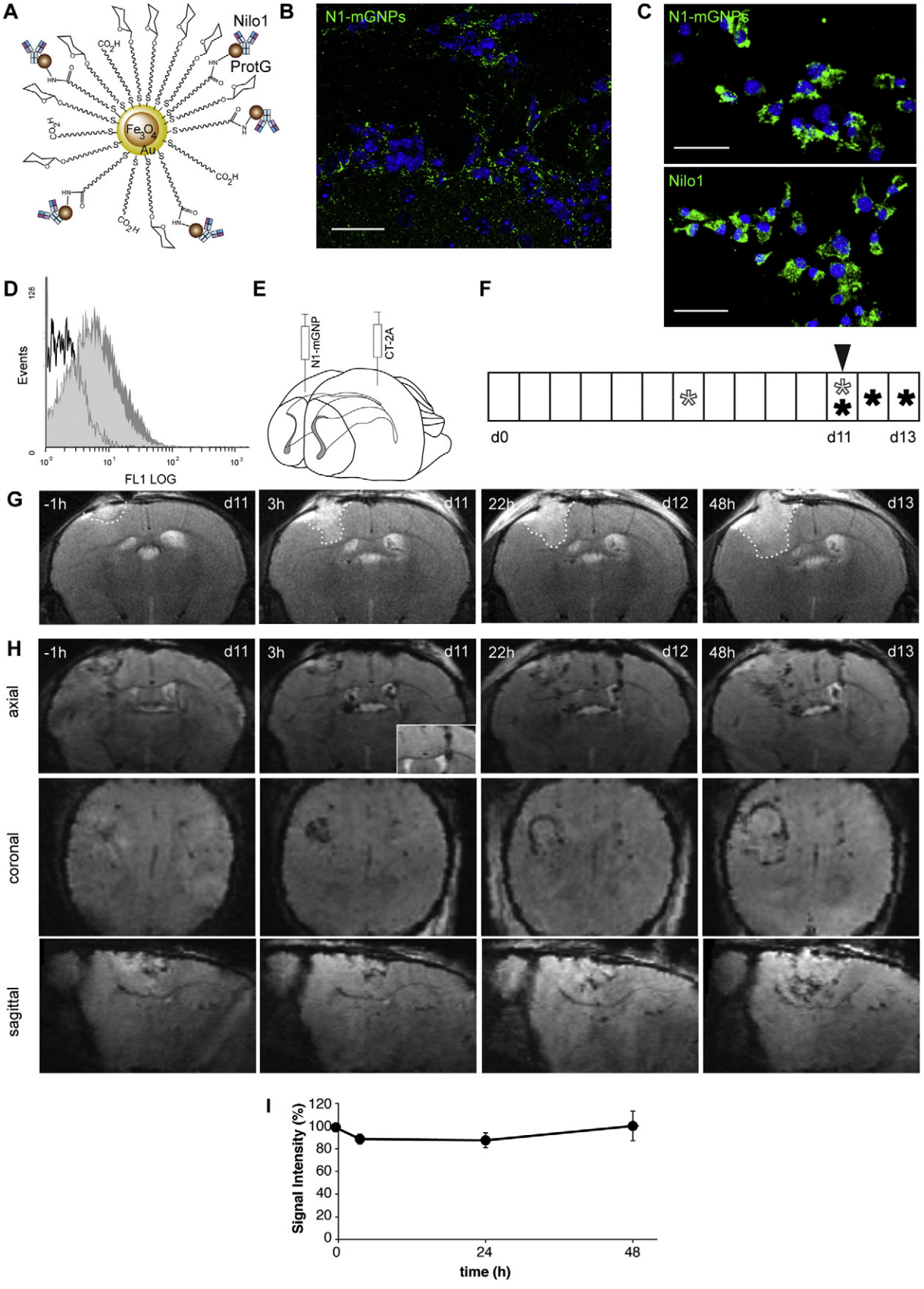

0.025% NaN_3). Following additional PBS washes, cells were resuspended in 300 μl cold PBS until FACS measurements (Epics XL, Coulter). Propidium iodine was added (25 μg/ml) to each sample to gate on living cells.

T2* MRI signal quantification

The accumulation of nanoparticles over time is reflected as an increase in the T2* hypointensity, equivalent to a drop in the overall intensity of the MRI signal. To evaluate the accumulation of nanoparticles, we measured signal intensity levels in the T2*-weighted images over time. For each animal, a region of interest (ROI) including the tumor area and its surroundings was manually delimited on the anatomical images (T2-weighted), at the final time point of the experiment. This ROI was translated to the T2*-weighed images (all images were previously co-registered) and the overall intensity value in the volume of interest was computed for each day of experiment on all the MRI sections. This processing was performed with the software MMWKS (Multimodality WorkStation) (Pascau et al., 2006). Signal intensity levels over time are expressed as percentage of the baseline T2* intensity for each animal and represented as mean ± S.D.

Results

Nilo1 mAb identifies type B astrocytes in the SVZ niche

Nilo antibodies were developed and characterized in our laboratory. Whereas Nilo2 mAb recognizes surface antigens expressed in neuroblasts, Nilo1 was described as identifying $Sox2^+$, $GFAP^+$, $vimentin^+$, $EGFR^+$, DCX^-, $PSA\text{-}NCAM^-$, and $Tuj1^-$ cells (Del Valle et al., 2010), suggesting that it identifies a highly undifferentiated neural precursor. Here we corroborated that Nilo1 recognized $Nestin^+$, $GFAP^+$ and $Sox2^+$ at the SVZ niche (Fig. 1A, Supplemental Fig. S1). The antigen recognized by Nilo1 mAb was not expressed in ependymal cells at the wall of the lateral ventricles ($CD24^+$) (Fig. 1B). In addition, $Nilo1^+$ cells did not correspond to type C cells (identified by a short pulse of BrdU and co-expressing high levels of Pax6 (Aguirre and Gallo, 2004; Kim et al., 2009; Parras et al., 2004)), since the $BrdU^+Pax6^{high}$ and the $Nilo1^+$ cells represented two distinct populations (Fig. 1B). As control, we show that a short pulse of BrdU did not label neuroblasts (Fig. 1B). Furthermore, Nilo1 identified different cell populations than Nilo 2 (Fig. 1C), excluding the possibility that Nilo1 recognized neuroblasts ($Nilo2^+$) (Del Valle et al., 2010). Moreover, the antigenic phenotype of $Nilo1^+$ cells allowed us to exclude that they could represent either intermediate progenitors such as NG2-glia, which are $GFAP^-$ (Dawson et al., 2003; Nishiyama et al., 2005), or differentiated astrocytes, since there is no Nilo1 signal in the brain cortex (Supplemental Fig. S2). Taken together, these data indicated that Nilo1 mAb identified surface antigens in SVZ-derived type B astrocytes, defined in adult mice as neural stem cells, since $Nilo1^+$ cells i) had a subependymal localization and did not recognize ependymal $CD24^+$ cells, ii) did not represent type C cells, iii) identified a population distinct from neuroblasts, iv) did not represent differentiated astrocytes nor intermediate progenitors NG2-glia like, and v) identified $SOX2^+$, $nestin^+GFAP^+$ cells. Further support to this notion came from the observation that on E10 mouse embryos, the radial glia markers vimentin and nestin (Mori et al., 2005) identified the same cells as Nilo1 (Fig. 1D and Supplemental Fig. S3).

In addition, we have been able to show that Nilo1 mAb recognized surface antigens in primary human glioblastoma cell lines growing as neurospheres (Fig. 1E and Supplemental Fig. S4). Indeed, we have analyzed 5 primary human glioblastoma cell lines, derived from 4 different patients and in all of them there were cells positively stained with Nilo1 mAb. These data indicate that this mAb is able to recognize, in addition to the mouse antigens against which they were raised, the homologous antigen in humans.

In vivo tracking of $Nilo1^+$ cells mobilized towards an induced glioblastoma

We have previously described, using protein G functionalized magnetic glyconanoparticles (mGNPs) bound to the monoclonal antibody Nilo2, that $Nilo2^+$ neuroblasts migrate towards an induced glioblastoma, and that this migration is ordered and fast (Elvira et al., 2012). In order to assess whether more undifferentiated precursors (type B cells) were also able to migrate to an induced tumor, we coupled Nilo1 mAb to the same mGNPs (Fig. 2A), which had been fully characterized elsewhere in terms of size core, shell composition, relaxivity and functionality (Elvira et al., 2012; Gallo et al., 2010; Gallo et al., 2011). Functionality of the Nilo1–mGNPs was evaluated by flow cytometry, immunocytochemistry and immunohistochemistry of the SVZ following *in vivo* injection of the Nilo1–mGNP particles (Figs. 2B–D). A stereotaxic graft of CT-2A astrocytoma cells (10^2–10^4 cells) into the left hemisphere (Fig. 2E) generated a highly reproducible glioblastoma at the injection site, which was followed by T2 magnetic resonance imaging (MRI) over time (Fig. 2F), demonstrating that it was grown on day 11 (Fig. 2G). At this time, Nilo1–mGNP complexes were intracranially injected by stereotaxic surgery into the right hemisphere (Figs. 2E, F) of anesthetized mice, which were subsequently imaged by MRI using T2* sequences (Fig. 2H). T2*-weighted MRI studies obtained 1 h before Nilo1–mGNP injection (d11, −1 h) were used as baseline for the experiment. To establish basal hypointensities on the MRI experiments several controls were made, including mice injected with PBS, to evaluate effects due to intracranial surgery (Supplemental Fig. S5 A,B); mice injected with CT-2A cells either alone (Supplemental Fig. S5 C,D) or in combination with an isotopic control antibody (CD3ε, developed in hamster) coupled to mGNPs, to evaluate signals due to either tumor growth or unspecific movement of mGNPs (Supplemental Fig. S5 E,F). None of this controls showed defined hypointense signals on T2*-weighted MRI studies.

The first T2*MRI study after Nilo1–mGNPs injection (d11, 3 h) allowed us to discard that the complexes were directly deposited in the cerebrospinal fluid (inset on Fig. 2H). At this time, in addition to black spots in the lateral ventricles, which corresponded to $Nilo1^+$ cells in their niches, we detected an increase in the signal hypointensities around the tumor, as compared with the baseline images (Fig. 2H d11, 3 h). These changes could not be explained by neo-vascularization during the four-hour lapse between MRIs. The hypointense T2* signals surrounding the tumor

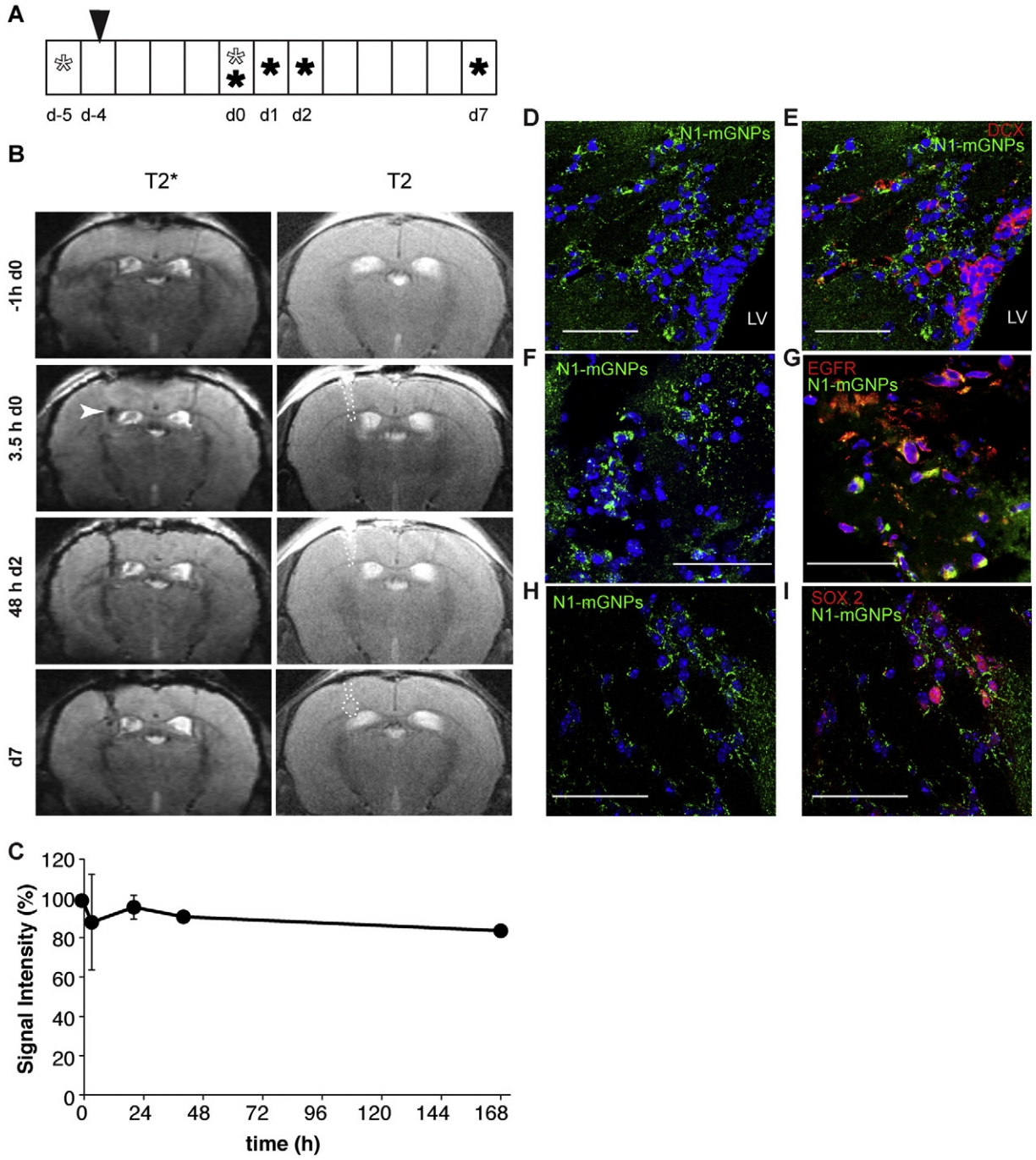

Figure 3 Migration of B astrocytes towards the tumor site occurs within hours following the insult. A, Experimental schedule where Nilo1–mGNPs injection day is indicated with an arrowhead and MRI acquisitions are shown with asterisks, before (empty) or after tumor cell injection at d0 (filled). B, Representative axial view from the experiment (n = 3) showing T2* MRI of a mouse injected with Nilo1–mGNPs (d4) and CT-2A cells (d0), analyzed just before (−1 h) or 3.5 h, 2 or 7 days after tumor injection (left column). T2 MRI analysis was used to follow tumor growth (right column). Arrowhead indicates hypointense signals accumulated just after tumor cell injection. C, Quantification of MRI signal intensity changes from B. The increase in the accumulation of nanoparticles surrounding the tumor is translated as a drop in the mean signal intensity in the region of interest. The controls are shown in Supplementary Fig. S4. D–I, Immunohistochemical analyses of fixed brains from mice analyzed by MRI either 24 h (D–G), or seven days (H, I) after the lesion. Nilo1$^+$ cells were detected by incubation with a secondary biotinylated anti-hamster Ig antibody and revealed with streptavidin A488. Double labeling with DCX (E), EGFR (G) or Sox2 (I). The MRI hypointense signals detected 3.5 h after tumor cell injection which are maintained and accumulated with time (up to 7 days) corresponded to Nilo1$^+$ cells which had arrived at the lesion site as undifferentiated B astrocytes. LV, lateral ventricle. Scale bars: 50 μm.

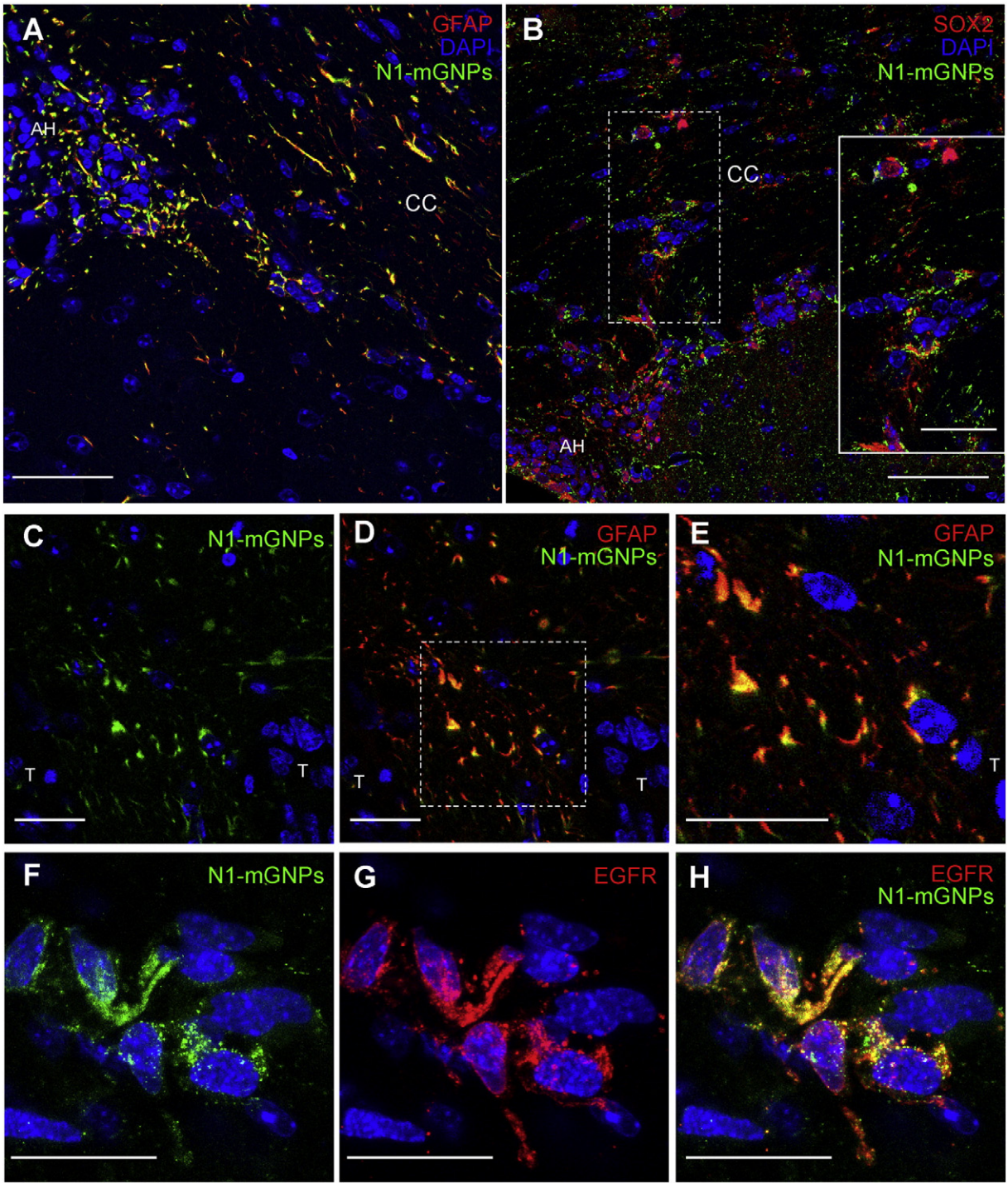

Figure 4 The MRI hypointense signals surrounding the tumor correspond to B astrocytes. Immunohistochemical analyses of fixed brains from mice analyzed in Fig. 2 two days after the Nilo1–mGNP injection (d13). Since Nilo1 mAb was already present in the Nilo1–mGNPs, Nilo1$^+$ cells were revealed by incubation with a secondary biotinylated anti-hamster Ig antibody and streptavidin-A488. A, B, SVZ ipsilateral to the Nilo1–mGNPs injection site demonstrating the presence of type B astrocytes (Nilo1$^+$ GFAP$^+$ or Nilo1$^+$Sox2$^+$) exiting the anterior horn (AH) of the lateral ventricle. C–H, Type B astrocytes were also present at the tumor site vicinity since they were Nilo1$^+$GFAP$^+$ (C–E) or Nilo1$^+$EGFR$^+$. F–H, Sites with MRI hypointense signals, indicating that Nilo1$^+$ cells migrated to the tumor site as B astrocytes. CC, *corpus callosum*; T, tumor. Scale bars: A–D, 50 μm; E–H and inset in B, 25 μm.

and additional hypointense signals between the niches and the lesion site accumulated over time (Fig. 2H, d12, d13), as quantified in Fig. 2I.

To discard that at longer experimental times, part of the hypointense signals could be due to neo-vascularization associated with tumor growth, we analyzed the Nilo1$^+$ cell

migration when the tumor mass was not yet formed (Fig. 3A). For this purpose, CT-2A cells were intracranially injected (d0) four days after Nilo1–mGNP injection (d4). Baseline T2*-weighted MRI images were taken 1 h prior to CT-2A injection, failing to detect any hypointense signal at the astrocytoma injection site (Fig. 3B, d0, −1 h). However, as soon as 3.5 h after injection of the CT-2A cells, an accumulation of hypointense spots at the cell injection site was detected (Fig. 3B, arrowhead d0, 3.5 h) in all analyzed mice. T2-weighted MRI studies (Fig. 3B) enabled the detection of the lesion produced by the stereotaxic injection of the needle to graft the tumor cells (d0, 3.5 h; d2) and the subsequent tumor formation (d7). An increase with time of hypointense signals (T2*-weighted MRI) was detected at this position (Figs. 2B, C) including the needle track (where CT-2A cells could have also been deposited) (d2), accumulating around the tumor when it was formed (d7). During these analyses, tumor-induced angiogenesis was undetectable, since in this glioblastoma model increases on days 12 to 14 (Fig. 2H, Supplemental Fig. S5 D, F).

To demonstrate that the hypointense signals detected by T2* MRI corresponded to Nilo1$^+$ cells, fixed tissues of the mice used in these MRI experiments were analyzed by immunohistochemistry. Since these tissue sections already contained Nilo1–mGNPs, the presence of Nilo1$^+$ cells was directly revealed with a fluorescently labeled specific secondary antibody.

In the experiments where Nilo1–mGNPs were injected before the CT-2A tumor cells, as soon as 24 h after the damage in the left *striatum*, we observed a SVZ thickening, concomitant with the presence of neuroblasts (DCX$^+$) and a high number of Nilo1$^+$ cells dispersed outside their usual subependymal location, infiltrating the adjacent striatum (Figs. 3D, E). This unusual location for Nilo1$^+$ cells, it could represent cells migrating from the lateral ventricle walls towards the adjacent parenchyma. In addition, *in vivo* labeled Nilo1$^+$ cells surrounding the lesion site were detected, confirming the MRI data (Fig. 3F). Moreover, Nilo1$^+$ cells were also EGFR$^+$, supporting the notion that these cells arrived undifferentiated at the lesion site (Fig. 3G). Even seven days after the damage, we still detected Nilo1$^+$ Sox2$^+$ cells between the niche and the damage site and surrounding the tumor (Figs. 3H, I).

These data were confirmed by immunohistochemistry analyses on the converse experiment where the CT-2A tumor was formed before the injection of the Nilo1–mGNPs, Nilo1$^+$ cells crossing the *corpus callosum* from the SVZ towards the lesion site were revealed 3 days after Nilo1–mGNP injection (13 days after tumor injection) (Figs. 4A, B). Conversely, on animals devoid of lesion, Nilo1$^+$ cells were circumscribed to the anterior horn and walls of the lateral ventricles (Fig. 1C) (Del Valle et al., 2010), showing the migration specificity of the labeled cells. In addition, Nilo1$^+$ cells expressed additional stem cell markers while migrating (GFAP$^+$SOX2$^+$) or even at the final destination surrounding the tumor (GFAP$^+$SOX2$^+$EGFR$^+$) (Fig. 4) suggesting that these cells migrated undifferentiated.

Migration of Nilo1$^+$ cells is a general trait for brain injury

To ascertain whether the migration of B astrocytes was restricted to the presence of tumor cells or rather to a more generalized response mechanism to brain damage, we analyzed for the presence of type B astrocytes in the neighborhood of three different kinds of brain injuries. Firstly we used a cryolesion model, which consists of applying dry ice over the left frontal bone for a short time. This model of brain injury generates an initial tissue damage which leads to secondary processes such as cell death, inflammation, vascular edema and blood–brain barrier disruption (Raslan et al., 2012). In this model Nilo1$^+$ cells were detected on the vicinity of the lesion three days after the injury by immunohistochemistry (Fig. 5A).

In a second lesion model, we induced a focal demyelinated lesion by lysolecithin (lysophosphatidilcholine, LPC) injection into the left *corpus callosum*. The initial LPC effect is a localized demyelination during the first week (Nait-Oumesmar et al., 1999) and maintenance of inflammatory signals during the second week (Cantarella et al., 2008). In these mice, seven days after LPC injection, the optimal time for the localized demyelinization, Nilo1$^+$ cell recruitment around the lesion site was detected (Fig. 5B) in sites containing GFAP$^+$ or Sox2$^+$ cells (data not shown). Furthermore, twenty-five days after LPC injection, when remyelination could be confirmed by the presence of O4$^+$ or myelin$^+$ cells, we also detected neuroblasts (Nilo2$^+$) adjacent to remyelinated cells (Fig. 5C).

The third injury model consisted of a cortical mechanical lesion induced by the puncture with a stereotaxic needle, where the damage site was revealed by injection of nigrosine. We could detect Nilo1$^+$ cells migrating to the damage site one to three days after the mechanical injury (Fig. 5D) in a location similar to that where neuroblasts were identified (Fig. 5E).

Migration of Nilo1$^+$ cells is associated with adult radial glia

Few hours after injuries produced by needle injection, the wound surrounding the needle track was filled by structures expressing Nilo1 (Fig. 6A). These processes might represent adult radial glia, since they express not only Nilo1 but also the glial marker GFAP, are associated to PSA-NCAM and to the erythrocyte markers Ter119$^+$, CD24$^+$, whereas did not represent reactive astrocytes since they were negative for vimentin and CD11b (Fig. 6B and data not shown).

Intraperitoneally injected Nilo1 mAb enables *in vivo* identification of brain glioblastomas

Since high grade brain tumors induce the blood–brain barrier breakdown (Wolburg et al., 2012), one week after intracranially injecting CT-2A-GFP cells, we administered intraperitoneally a single dose of Nilo1 mAb (10 μg/g of body weight) and sacrificed the mice the next day. In the fixed brains, the presence of Nilo1 was revealed by immunohistochemistry with a fluorescently labeled secondary antibody, demonstrating the presence of type B cells surrounding the GFP$^+$ glioblastoma cells (Fig. 7A). The use of GFP tumor cells allowed us the identification of host cells (Nilo1$^+$ GFP$^-$, arrowheads in Fig. 7B) in areas where isolated tumor cells infiltrated the parenchyma. This experiment corroborated the notion that type B astrocytes migrate towards the tumor site and opens up the possibility of using

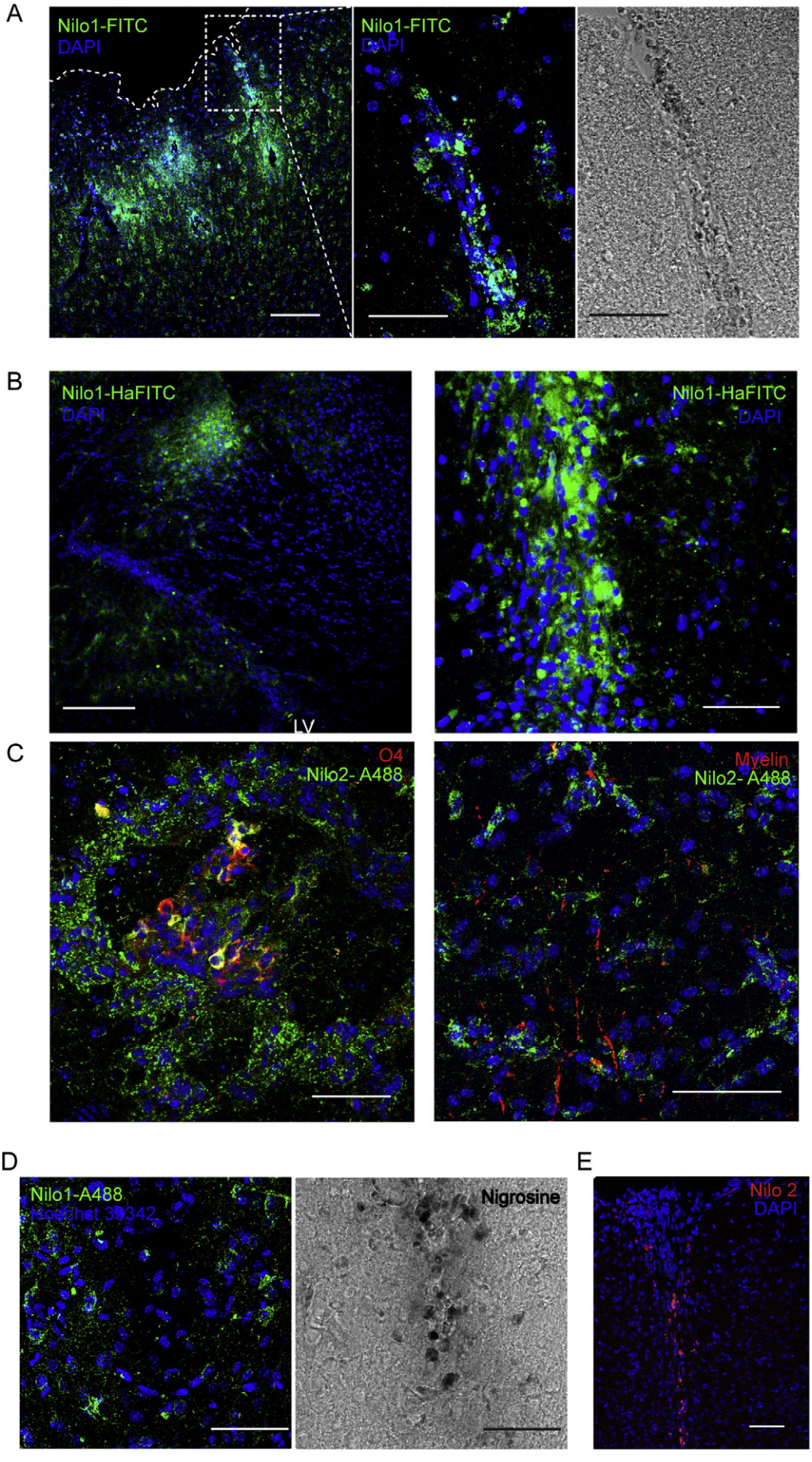
A
Nilo1-FITC
DAPI
Nilo1-FITC
DAPI
B
Nilo1-HaFITC
DAPI
LV
Nilo1-HaFITC
DAPI
C
O4
Nilo2- A488
Myelin
Nilo2- A488
D
Nilo1-A488
Hoechst 33342
Nigrosine
E
Nilo 2
DAPI

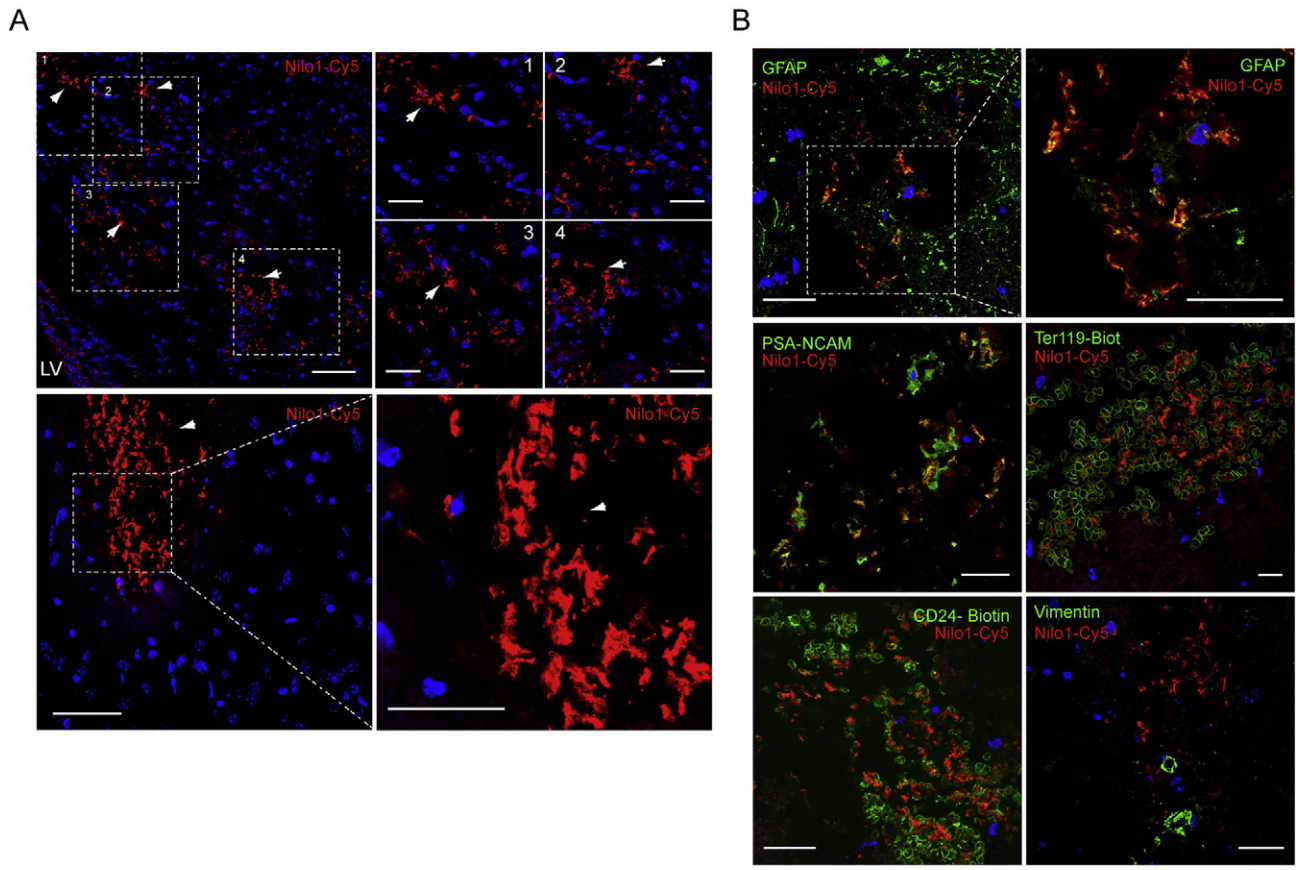

Figure 6 GFAP$^+$ Nilo1$^+$ processes coalesced and filled the damaged tissue. A, Immunohistochemical analyses of fixed brains from the needle track site on mice intracranially injected with CT-2A cells (top row) (n = 3) or PBS (bottom row) (n = 3) and analyzed by confocal microscopy 24 h after the lesion. Staining with Nilo1-Cy5 allows detection, in addition to Nilo1$^+$ cells from SVZ towards the lesion site, of processes that at these early times fill the broken tissue (arrowheads). B, Double immunohistochemistry staining of fixed brains from mice injected with PBS 24 h before, demonstrating that these Nilo1$^+$ processes were compatible with adult radial glia since they were Nilo1$^+$GFAP$^+$, where associated with PSA-NCAM$^+$ structures and red blood cells Ter-119$^+$, CD24$^+$. These processes did not represent reactive astrocytes since they were vimentin$^-$. LV, lateral ventricle. Scale bars: A, left panels 50 μm, right panels 25 μm; B, 25 μm.

intraperitoneally injected antibodies to follow brain damage in situations where the blood–brain barrier is disrupted.

Discussion

Although there are evidences that immature neurons present in brain lesion sites, such as peri-infarcted tissue, come from GFAP$^+$ SVZ-derived neural stem cells (Garcia et al., 2004; Ohab and Carmichael, 2008; Ohab et al., 2006), a direct mobilization of type B astrocytes towards a lesion site has not yet been reported.

To study the migration of early neural progenitors towards a brain injury, we used Nilo1 mAb. Here we demonstrate that Nilo1 identified type B astrocytes (or adult neural stem cells) since i) it recognized GFAP$^+$, Sox2$^+$ and EGFR$^+$ cells, being negative for the neuroblast markers

Figure 5 Migration of B astrocytes occurred following several types of injury. Immunohistochemistry of fixed brains analyzed by confocal microscopy. A, Three days after a cryolesion, Nilo1$^+$ cells were present surrounding the lesion site (dotted line, left panel); magnification showing fluorescent (middle) or bright field (right panel) microscopy where Nilo1$^+$ cells were associated to blood vessels (n = 5). B, Seven days following a demyelination, Nilo1$^+$ cells were found between the niche (LV) and the lesion site (left panel) where they accumulated (right panel) (n = 3). C, This movement of Nilo1$^+$ cells was followed by the appearance of O4$^+$ and myelin$^+$ cells 25 days after demyelination (n = 3). D, Three days after a mechanical damage produced by stereotaxic injection of PBS (n = 6), Nilo1$^+$ cells were detected surrounding the lesion site (left panel) revealed by nigrosine (right panel) on a bright field microscopy. E, Three days after a mechanical damage produced by stereotaxic injection of PBS, Nilo2$^+$ neuroblasts were detected filling the lesion site. Scale bars: A and B left panels, 150 μm; A, central and right panels; B right panel, C–E, 50 μm.

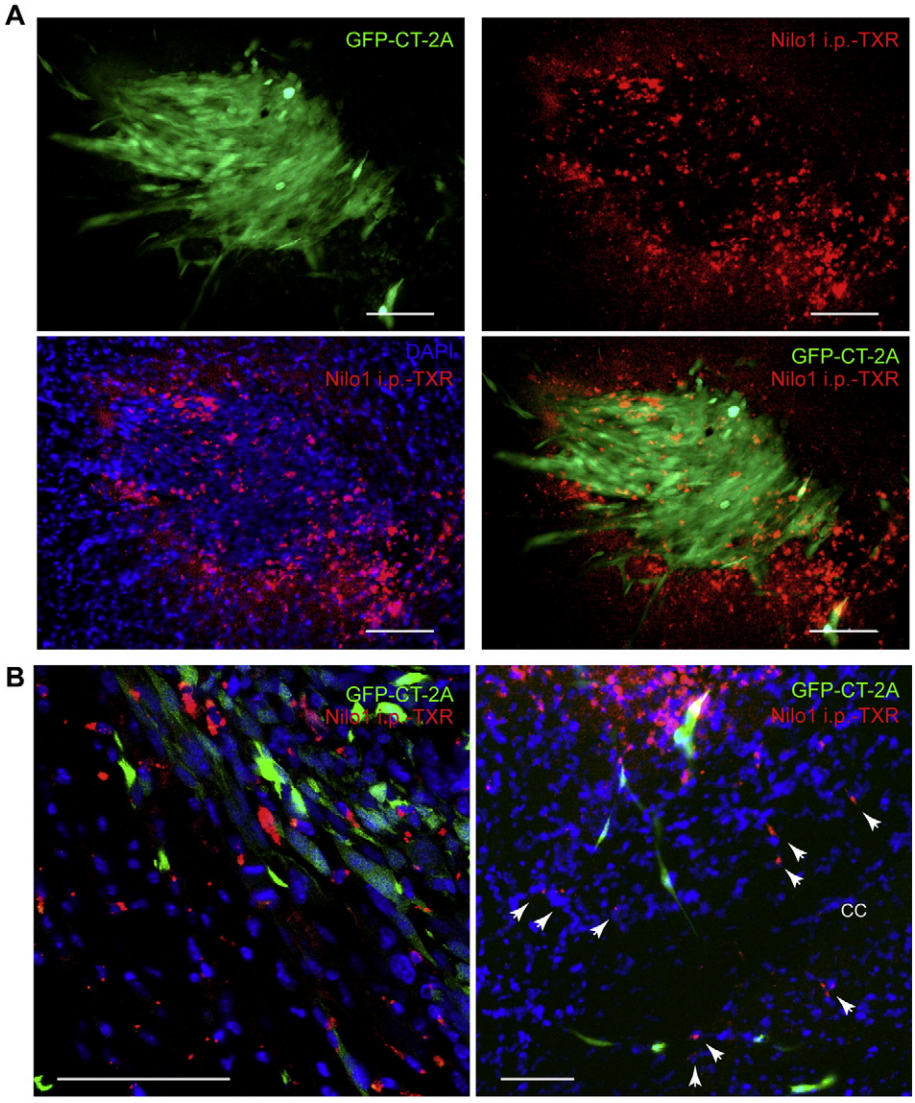

Figure 7 *In vivo* identification of B astrocytes surrounding a brain tumor after intraperitoneal injection of the Nilo1 mAb. Immunohistochemical analyses of fixed brain from mice injected with GFP-CT-2A cells (GFP^+ in green) in the left *striatum*, in which Nilo1 was intraperitoneally injected one week after tumor cell injection, and mice (n = 4) sacrificed 24 h later. A, Low and B, high magnification showing that $Nilo1^+$ cells surrounding the tumor were host-derived (left panel). An accumulation of $Nilo1^+$ cells was detected surrounding infiltrated tumor cells (right panel). $Nilo1^+$ cells (red) were revealed with anti-hamster Cy5.5. Scale bars: A, 100 μm; B, 75 μm.

DCX and Nilo2; ii) Nilo1 did not stain ependymal $CD24^+$ cells, having instead subependymal localization on the SVZ; iii) transient amplifying cells (or type C cells, which are $Pax6^{high}BrdU^+$ on tissue sections from *in vivo* labeled animals with a short BrdU pulse) (Aguirre and Gallo, 2004; Kim et al., 2009; Parras et al., 2004) and $Nilo1^+$ cells represented two distinct populations; iv) $Nilo1^+$ cells were $GFAP^+$, excluding the possibility that this mAb identified intermediate progenitors in the differentiation process, like NG2-precursors which are $GFAP^-$ (Dawson et al., 2003; Nishiyama et al., 2005); v) double staining of E10 embryo brains with Nilo1 and either vimentin or nestin suggested that Nilo1 recognizes embryonic radial glia.

Nilo1 mAb, coupled to functionalized magnetic nanoparticles in combination with magnetic resonance imaging allowed us to identify the $Nilo1^+$ cells at their niche in the SVZ and, in animals carrying a lesion, at intermediate positions between the niche and the lesion site, where they accumulated over time. The migratory response was very fast since MRI hypointense signals at the lesion site were detected by MRI 3 h after injection of the Nilo1–mGNP complexes in animals bearing tumors, or 3.5 h after injection of the CT-2A cells on animals that had previously been injected with Nilo1–mGNP complexes. The presence of $Nilo1^+$ cells at the lesion site was corroborated by immunohistochemistry analyses on fixed brain sections from these mice, incubating with a fluorescent secondary antibody, since the $Nilo1^+$ cells were already labeled *in vivo* with the Nilo1–mGNPs. Immunohistochemistry confirmed not only that the hypointense signals corresponded to $Nilo1^+$ cells

surrounding the tumor, but also that these cells retained their type B astrocyte phenotype (GFAP$^+$, EGFR$^+$, Sox2$^+$) following their migration.

The migration of adult neural stem cells (type B astrocytes) towards a tumor site, rather than a tumor-specific response, turned out to be a more generalized response to brain insults since we detected Nilo1$^+$ cells at the sites where other types of lesions were produced (*i.e.* cryolesion, demyelination, mechanical injury). These lesions were chosen because they are very different from each other and from the tumor implantation model described above. In all of them, Nilo1$^+$ cells were detected surrounding the lesions, although we cannot formally exclude at this time that some of the Nilo1$^+$ cells surrounding the lesion represent cells around the injury site de novo expressing Nilo1 upon injury.

In addition to Nilo1$^+$ cells migrating to the lesion sites, both in a mechanical lesion model and after any stereotactic injection, we detected, one day after the lesion, coalescing structures filling the wound-lesion that expressed high levels of Nilo1 antigen. These Nilo1$^+$ processes were GFAP$^+$, vimentin$^-$ and CD11b$^-$, forming structures associated to PSA-NCAM. On the one hand, the observation that these structures did not express vimentin or CD11b allowed us to exclude that they represented proximal reactive astrocytes (Holmin et al., 1997; Raedt et al., 2009; Ridet et al., 1997; Robel et al., 2011). On the other hand, their GFAP$^+$ staining was compatible with the presence of adult radial glia fibers or glial tubes. In physiological conditions they have been described to support the migration of neuroblasts either towards the olfactory bulb (Doetsch and Alvarez-Buylla, 1996; Ohab and Carmichael, 2008; Yang et al., 2005), acting as substrate for the migrating progenitor cells after focal apoptosis in the adult brain (Leavitt et al., 1999), or from their proliferation zones to the lesion sites in adult brain in fish (Clint and Zupanc, 2001; Zupanc and Clint, 2003). The appearance of fibers either from astrocytes or adult radial glia emanating from their SVZ subependymal position has also been described not only under physiological conditions (Kriegstein and Alvarez-Buylla, 2009; Thored et al., 2006; Teramoto et al., 2003), but also in rodent or fish brain lesions (Thored et al., 2006; Holmin et al., 1997; Ohab and Carmichael, 2008; Clint and Zupanc, 2001; Zupanc and Clint, 2003; Szele and Chesselet, 1996). Radial glia cells have been defined as neuronal precursors (Robel et al., 2011; Noctor et al., 2001; Malatesta et al., 2000) and it has been suggested that they could represent a specific subpopulation of astrocytes in adult mammals (Kriegstein and Alvarez-Buylla, 2009; Robel et al., 2011; Noctor et al., 2001; Malatesta et al., 2000; Gubert et al., 2009). Furthermore, the presence of radial glia in adult hippocampus where neurogenesis occurs throughout life, or in non-mammalian vertebrates where neurogenesis persists in a rather wide-spread fashion in the adult brain (Clint and Zupanc, 2001; Pinto and Gotz, 2007), raise the possibility that the neurogenic potential of radial glia may extend into adulthood in some brain regions (Noctor et al., 2001) or even as an acute response to brain lesions, were neurogenesis is necessary and commonly associated to brain tissue repairing processes.

Interestingly, the migration kinetics of type B astrocytes was similar to that previously described for neuroblasts (Elvira et al., 2012). This suggests that both cell types are able to respond to the same "damage signals" and that type B astrocytes could help in neuroblast migration as previously suggested from *in vitro* (Song et al., 2002; Lim and Alvarez-Buylla, 1999) or *in vivo* data (Kriegstein and Alvarez-Buylla, 2009; Leavitt et al., 1999; Noctor et al., 2001; Alvarez-Buylla and Nottebohm, 1988). Nilo1$^+$ radial glia-like processes reported here support the notion that radial glia is a mainstay for neurogenesis not only during the embryonic stage but also during adulthood.

The migration of neural stem cells reported here is fully in accordance with data showing that stimulation with exogenous growth factors increase cell proliferation at the SVZ and promote the migration of SVZ-derived cells into the adjacent parenchyma or even at the vicinity of a brain lesion site (Cantarella et al., 2008; Teramoto et al., 2003; Craig et al., 1996; Doetsch et al., 2002; Gonzalez-Perez et al., 2009). Growth factor infusions also increased the number of GFAP$^+$ cells exhibiting long processes that link the ischemic *striatum* to the SVZ niche (Teramoto et al., 2003). The lesion it self induces the secretion of growth and trophic factors (Sundholm-Peters et al., 2005; Goings et al., 2004; Ridet et al., 1997; Suzuki et al., 2012) that could activate quiescent precursors (Ridet et al., 1997) or modify astrocyte morphology (Junier, 2000) resulting in the mobilization SVZ-derived cells.

Finally, by definition of the experimental procedures presented here, the positions where the grafted tumors will grow are already known, and therefore cannot be used from the diagnostic point of view, the data presented here represent a proof of concept that MRI using Nilo1–mGNPs could be used in humans for detection of brain primary tumors or recidives very early on, before contrast substances such as gadolinium would give a detectable signal, in particular since we have been able to show that Nilo1 mAb is able to identify the corresponding antigens present in human glioblastoma derived cells.

Conclusions

In summary, our data show that by combining Nilo1, a monoclonal antibody able to identify surface antigens in type B astrocytes and radial glia during development, with superparamagnetic nanoparticles, the adult neural stem cells can be identified in their niches and follow their fast and orderly migration towards a lesion site *in vivo* using MRI. Furthermore, the migration of these cells towards a lesion site seems to be a general trait, since it can be detected during development of a tumor, following a cryolesion, demyelination or even a mechanical injury, generating in addition few hours after the damage radial glia-like structures at the lesion site.

Supplementary data to this article can be found online at http://dx.doi.org/10.1016/j.scr.2014.11.006.

Acknowledgments

This work was supported by grants from the Instituto de Salud Carlos III (grant RD06/0010/1010 to JAGS), and the Ministry of Science and Innovation (grants SAF2009-07974 to JAGS, CTQ-2011-271268 to SP, AMIT, CENIT-CDTI to MD). We would like to thank

Prof. T.N. Syfried, Boston, MA, USA and Dr. A. Martinez (I. Cajal, Madrid, Spain) for providing CT-2A and GFP-CT-2A cells respectively. Dr. L. Kremer (ProteinTools, CNB-CSIC, Madrid, Spain) for help and advice on mAb purification and labeling. We are grateful to M.T. Seisdedos and to the CIB animal and confocal microscopy facilities.

References

Aguirre, A., Gallo, V., 2004. Postnatal neurogenesis and gliogenesis in the olfactory bulb from NG2-expressing progenitors of the subventricular zone. J. Neurosci. 24, 10530–10541.

Alonso, G., Prieto, M., Chauvet, N., 1999. Tangential migration of young neurons arising from the subventricular zone of adult rats is impaired by surgical lesions passing through their natural migratory pathway. J. Comp. Neurol. 405, 508–528.

Alvarez-Buylla, A., Nottebohm, F., 1988. Migration of young neurons in adult avian brain. Nature 335, 353–354.

Arvidsson, A., Collin, T., Kirik, D., et al., 2002. Neuronal replacement from endogenous precursors in the adult brain after stroke. Nat. Med. 8, 963–970.

Bonfanti, L., Peretto, P., 2007. Radial glial origin of the adult neural stem cells in the subventricular zone. Prog. Neurobiol. 83, 24–36.

Cantarella, C., Cayre, M., Magalon, K., et al., 2008. Intranasal HB-EGF administration favors adult SVZ cell mobilization to demyelinated lesions in mouse corpus callosum. Dev. Neurobiol. 68, 223–236.

Clint, S.C., Zupanc, G.K., 2001. Neuronal regeneration in the cerebellum of adult teleost fish, *Apteronotus leptorhynchus*: guidance of migrating young cells by radial glia. Brain Res. Dev. Brain Res. 130, 15–23.

Craig, C.G., Tropepe, V., Morshead, C.M., et al., 1996. In vivo growth factor expansion of endogenous subependymal neural precursor cell populations in the adult mouse brain. J. Neurosci. 16, 2649–2658.

Dawson, M.R., Polito, A., Levine, J.M., et al., 2003. NG2-expressing glial progenitor cells: an abundant and widespread population of cycling cells in the adult rat CNS. Mol. Cell. Neurosci. 24, 476–488.

Del Valle, I., Elvira, G., Garcia-Benzaquen, L., et al., 2010. Characterization of novel monoclonal antibodies able to identify neurogenic niches and arrest neurosphere proliferation and differentiation. Neuroscience 169, 1473–1485.

Doetsch, F., Alvarez-Buylla, A., 1996. Network of tangential pathways for neuronal migration in adult mammalian brain. Proc. Natl. Acad. Sci. U. S. A. 93, 14895–14900.

Doetsch, F., Caille, I., Lim, D.A., et al., 1999. Subventricular zone astrocytes are neural stem cells in the adult mammalian brain. Cell 97, 703–716.

Doetsch, F., Petreanu, L., Caille, I., et al., 2002. EGF converts transit-amplifying neurogenic precursors in the adult brain into multipotent stem cells. Neuron 36, 1021–1034.

Elvira, G., Garcia, I., Benito, M., et al., 2012. Live imaging of mouse endogenous neural progenitors migrating in response to an induced tumor. PLoS One 7, e44466.

Gallo, J., García, I., Padro, D., et al., 2010. Water-soluble magnetic glyconanoparticles based on metal-doped ferrites coated with gold: Synthesis and characterization. J. Mater. Chem. 20, 10010.

Gallo, J., García, I., Genicio, N., et al., 2011. Specific labelling of cell populations in blood with targeted immuno-fluorescent/magnetic glyconanoparticles. Biomaterials 32, 9818–9825.

Garcia, A.D., Doan, N.B., Imura, T., et al., 2004. GFAP-expressing progenitors are the principal source of constitutive neurogenesis in adult mouse forebrain. Nat. Neurosci. 7, 1233–1241.

García, I., Gallo, J., Genicio, N., et al., 2011. Magnetic glyconanoparticles as a versatile platform for selective immunolabeling and imaging of cells. Bioconjug. Chem. 22, 264–273.

Glass, R., Synowitz, M., Kronenberg, G., et al., 2005. Glioblastoma-induced attraction of endogenous neural precursor cells is associated with improved survival. J. Neurosci. 25, 2637–2646.

Goings, G.E., Sahni, V., Szele, F.G., 2004. Migration patterns of subventricular zone cells in adult mice change after cerebral cortex injury. Brain Res. 996, 213–226.

Gonzalez-Perez, O., Romero-Rodriguez, R., Soriano-Navarro, M., et al., 2009. Epidermal growth factor induces the progeny of subventricular zone type B cells to migrate and differentiate into oligodendrocytes. Stem Cells 27, 2032–2043.

Gotts, J.E., Chesselet, M.F., 2005. Migration and fate of newly born cells after focal cortical ischemia in adult rats. J. Neurosci. Res. 80, 160–171.

Gubert, F., Zaverucha-do-Valle, C., Pimentel-Coelho, P.M., et al., 2009. Radial glia-like cells persist in the adult rat brain. Brain Res. 1258, 43–52.

Holmin, S., Almqvist, P., Lendahl, U., et al., 1997. Adult nestin-expressing subependymal cells differentiate to astrocytes in response to brain injury. Eur. J. Neurosci. 9, 65–75.

Jankovski, A., Garcia, C., Soriano, E., et al., 1998. Proliferation, migration and differentiation of neuronal progenitor cells in the adult mouse subventricular zone surgically separated from its olfactory bulb. Eur. J. Neurosci. 10, 3853–3868.

Junier, M.P., 2000. What role(s) for TGFalpha in the central nervous system? Prog. Neurobiol. 62, 443–473.

Kim, Y., Comte, I., Szabo, G., et al., 2009. Adult mouse subventricular zone stem and progenitor cells are sessile and epidermal growth factor receptor negatively regulates neuroblast migration. PLoS One 4, e8122.

Kriegstein, A., Alvarez-Buylla, A., 2009. The glial nature of embryonic and adult neural stem cells. Annu. Rev. Neurosci. 32, 149–184.

Leavitt, B.R., Hernit-Grant, C.S., Macklis, J.D., 1999. Mature astrocytes transform into transitional radial glia within adult mouse neocortex that supports directed migration of transplanted immature neurons. Exp. Neurol. 157, 43–57.

Lim, D.A., Alvarez-Buylla, A., 1999. Interaction between astrocytes and adult subventricular zone precursors stimulates neurogenesis. Proc. Natl. Acad. Sci. U. S. A. 96, 7526–7531.

Lois, C., Alvarez-Buylla, A., 1994. Long-distance neuronal migration in the adult mammalian brain. Science 264, 1145–1148.

Lois, C., Garcia-Verdugo, J.M., Alvarez-Buylla, A., 1996. Chain migration of neuronal precursors. Science 271, 978–981.

Malatesta, P., Hartfuss, E., Gotz, M., 2000. Isolation of radial glial cells by fluorescent-activated cell sorting reveals a neuronal lineage. Development 127, 5253–5263.

Martinez-Murillo, R., Martinez, A., 2007. Standardization of an orthotopic mouse brain tumor model following transplantation of CT-2A astrocytoma cells. Histol. Histopathol. 22, 1309–1326.

Mirzadeh, Z., Merkle, F.T., Soriano-Navarro, M., et al., 2008. Neural stem cells confer unique pinwheel architecture to the ventricular surface in neurogenic regions of the adult brain. Cell Stem Cell 3, 265–278.

Mori, T., Buffo, A., Gotz, M., 2005. The novel roles of glial cells revisited: the contribution of radial glia and astrocytes to neurogenesis. Curr. Top. Dev. Biol. 69, 67–99.

Nait-Oumesmar, B., Decker, L., Lachapelle, F., et al., 1999. Progenitor cells of the adult mouse subventricular zone proliferate, migrate and differentiate into oligodendrocytes after demyelination. Eur. J. Neurosci. 11, 4357–4366.

Nakatomi, H., Kuriu, T., Okabe, S., et al., 2002. Regeneration of hippocampal pyramidal neurons after ischemic brain injury by recruitment of endogenous neural progenitors. Cell 110, 429–441.

Nam, S.C., Kim, Y., Dryanovski, D., et al., 2007. Dynamic features of postnatal subventricular zone cell motility: a two-photon time-lapse study. J. Comp. Neurol. 505, 190–208.

Nishiyama, A., Yang, Z., Butt, A., 2005. Astrocytes and NG2-glia: what's in a name? J. Anat. 207, 687–693.

Noctor, S.C., Flint, A.C., Weissman, T.A., et al., 2001. Neurons derived from radial glial cells establish radial units in neocortex. Nature 409, 714–720.

Ohab, J.J., Carmichael, S.T., 2008. Poststroke neurogenesis: emerging principles of migration and localization of immature neurons. Neuroscientist 14, 369–380.

Ohab, J.J., Fleming, S., Blesch, A., et al., 2006. A neurovascular niche for neurogenesis after stroke. J. Neurosci. 26, 13007–13016.

Palmer, T.D., Takahashi, J., Gage, F.H., 1997. The adult rat hippocampus contains primordial neural stem cells. Mol. Cell. Neurosci. 8, 389–404.

Parras, C.M., Galli, R., Britz, O., et al., 2004. Mash1 specifies neurons and oligodendrocytes in the postnatal brain. EMBO J. 23, 4495–4505.

Pascau, J., Vaquero, J., Abella, M., et al., 2006. Multimodality workstation for small animal image visualization and analysis. Scientific Papers. Mol. Imaging Biol. 8, 97–98.

Peters, A.A., Palay, S.L., Webster, H.D., 1991. The Fine Structure of the Nervous System: Neurons and Their Supporting Cells. Oxford University Press, New York.

Picard-Riera, N., Decker, L., Delarasse, C., et al., 2002. Experimental autoimmune encephalomyelitis mobilizes neural progenitors from the subventricular zone to undergo oligodendrogenesis in adult mice. Proc. Natl. Acad. Sci. U. S. A. 99, 13211–13216.

Pinto, L., Gotz, M., 2007. Radial glial cell heterogeneity—the source of diverse progeny in the CNS. Prog. Neurobiol. 83, 2–23.

Raedt, R., Van Dycke, A., Van Melkebeke, D., et al., 2009. Seizures in the intrahippocampal kainic acid epilepsy model: characterization using long-term video-EEG monitoring in the rat. Acta Neurol. Scand. 119, 293–303.

Raslan, F., Albert-Weissenberger, C., Ernestus, R.I., et al., 2012. Focal brain trauma in the cryogenic lesion model in mice. Exp. Transl. Stroke Med. 4, 6.

Reynolds, B.A., Weiss, S., 1992. Generation of neurons and astrocytes from isolated cells of the adult mammalian central nervous system. Science 255, 1707–1710.

Richards, L.J., Kilpatrick, T.J., Bartlett, P.F., 1992. De novo generation of neuronal cells from the adult mouse brain. Proc. Natl. Acad. Sci. U. S. A. 89, 8591–8595.

Ridet, J.L., Malhotra, S.K., Privat, A., et al., 1997. Reactive astrocytes: cellular and molecular cues to biological function. Trends Neurosci. 20, 570–577.

Robel, S., Berninger, B., Gotz, M., 2011. The stem cell potential of glia: lessons from reactive gliosis. Nat. Rev. Neurosci. 12, 88–104.

Song, H., Stevens, C.F., Gage, F.H., 2002. Astroglia induce neurogenesis from adult neural stem cells. Nature 417, 39–44.

Sundholm-Peters, N.L., Yang, H.K., Goings, G.E., et al., 2004. Radial glia-like cells at the base of the lateral ventricles in adult mice. J. Neurocytol. 33, 153–164.

Sundholm-Peters, N.L., Yang, H.K., Goings, G.E., et al., 2005. Subventricular zone neuroblasts emigrate toward cortical lesions. J. Neuropathol. Exp. Neurol. 64, 1089–1100.

Suzuki, T., Sakata, H., Kato, C., et al., 2012. Astrocyte activation and wound healing in intact-skull mouse after focal brain injury. Eur. J. Neurosci. 1–12.

Szele, F.G., Chesselet, M.F., 1996. Cortical lesions induce an increase in cell number and PSA-NCAM expression in the subventricular zone of adult rats. J. Comp. Neurol. 368, 439–454.

Teramoto, T., Qiu, J., Plumier, J.C., et al., 2003. EGF amplifies the replacement of parvalbumin-expressing striatal interneurons after ischemia. J. Clin. Invest. 111, 1125–1132.

Thored, P., Arvidsson, A., Cacci, E., et al., 2006. Persistent production of neurons from adult brain stem cells during recovery after stroke. Stem Cells 24, 739–747.

Wolburg, H., Noell, S., Fallier-Becker, P., et al., 2012. The disturbed blood–brain barrier in human glioblastoma. Mol. Aspects Med. 33, 579–589.

Yang, P., Baker, K.A., Hagg, T., 2005. A disintegrin and metalloprotease 21 (ADAM21) is associated with neurogenesis and axonal growth in developing and adult rodent CNS. J. Comp. Neurol. 490, 163–179.

Zupanc, G.K., Clint, S.C., 2003. Potential role of radial glia in adult neurogenesis of teleost fish. Glia 43, 77–86.